

ARTICLE OPEN



Jumonji histone demethylases are therapeutic targets in small cell lung cancer

Aiden Nguyen¹, Clarissa G. Nuñez¹, Tram Anh Tran¹, Luc Girard^{1,2}, Michael Peyton¹, Rodrigo Catalan¹, Cristina Guarena¹, Kimberley Avila¹, Benjamin J. Drapkin^{1,3,4}, Raghav Chandra^{1,5}, John D. Minna^{1,2,3,4} and Elisabeth D. Martinez^{1,2,4}✉

© The Author(s) 2024

Small cell lung cancer (SCLC) is a recalcitrant cancer of neuroendocrine (NE) origin. Changes in therapeutic approaches against SCLC have been lacking over the decades. Here, we use preclinical models to identify a new therapeutic vulnerability in SCLC consisting of the targetable Jumonji lysine demethylase (KDM) family. We show that Jumonji demethylase inhibitors block malignant growth and that etoposide-resistant SCLC cell lines are particularly sensitive to Jumonji inhibition. Mechanistically, small molecule-mediated inhibition of Jumonji KDMs activates endoplasmic reticulum (ER) stress genes, upregulates ER stress signaling, and triggers apoptotic cell death. Furthermore, Jumonji inhibitors decrease protein levels of SCLC NE markers INSM1 and Secretogranin-3 and of driver transcription factors ASCL1 and NEUROD1. Genetic knockdown of KDM4A, a Jumonji demethylase highly expressed in SCLC and a known regulator of ER stress genes, induces ER stress response genes, decreases INSM1, Secretogranin-3, and NEUROD1 and inhibits proliferation of SCLC in vitro and in vivo. Lastly, we demonstrate that two different small molecule Jumonji KDM inhibitors (pan-inhibitor JIB-04 and KDM4 inhibitor SD70) block the growth of SCLC tumor xenografts in vivo. Our study highlights the translational potential of Jumonji KDM inhibitors against SCLC, a clinically feasible approach in light of recently opened clinical trials evaluating this drug class, and establishes KDM4A as a relevant target across SCLC subtypes.

Oncogene (2024) 43:2885–2899; <https://doi.org/10.1038/s41388-024-03125-x>

INTRODUCTION

Small cell lung cancer (SCLC) is an aggressive neuroendocrine malignancy with poor prognosis because of rapid growth, early development of metastases, and acquired drug resistance [1]. Recently, immune checkpoint blockade immunotherapy has been approved for standard treatment with platin/etoposide, along with lurbinectedin for second-line treatment, yet overall median survival remains under 12 months, and therapy has changed little over several decades despite ongoing clinical trials to test new strategies [2–6]. Among all lung cancers, SCLC uniquely expresses high levels of neuroendocrine (NE) lineage transcription factors, including ASCL1 and/or NEUROD1 [5, 6]. Both of these lineage transcription factors promote the development and growth of neuroendocrine cells and have been shown to augment tumor growth and migration in SCLC [7, 8]. In addition, distinct subsets of SCLC are driven by other factors including POU2F3 [9–12], although these are uncommon. SCLC tumors have a high mutational burden, almost universal loss of function of tumor suppressor genes *RB1* and *TP53*, with the vast majority of patients having long-term exposure to tobacco carcinogens [12, 13].

Platinum-etoposide chemotherapy has been the first-line treatment of SCLC since 1980 [14]. Although in most patients this chemotherapy initially gives clinical and survival benefit, patients nearly always relapse with acquired chemoresistance [14, 15]. Unfortunately, only 20% of patients respond to second-

line topotecan therapy, emphasizing the need to identify new treatment alternatives [16]. In an effort to address this key knowledge gap, the National Cancer Institute evaluated 103 FDA-approved oncology drugs and 423 investigational agents in tests of a large panel of patient-derived SCLC cell lines. While there were large differences in response phenotypes (drug IC₅₀ values) of individual SCLCs across the drug panel, in all cases these were highly and positively correlated with sensitivity or resistance to etoposide, part of standard platin/etoposide front-line therapy [14]. Since this study, novel small molecules have been developed by our group and others to test the effect of modulating epigenetic pathways by blocking the action of the Jumonji lysine demethylase (KDM) family members [17–21]. Yet these have not been evaluated against SCLC.

The involvement and upregulation of Jumonji KDM enzymes in malignancy and therapeutic resistance is broadly appreciated due to their unique ability to erase trimethyl regulatory marks on histone tails and reprogram the transcriptome, yet little is known about the role of these demethylases in SCLC. Supporting the notion that Jumonji KDMs may be essential for SCLC survival, both a CRISPR and an independent RNAi genetic dropout screen on a small panel of SCLC cell lines implicated several Jumonji KDMs as necessary for SCLC growth [22, 23]. In addition, the Kaelin laboratory subsequently found that Jumonji KDM5A promotes SCLC proliferation by maintaining ASCL1 activity through

¹Hamon Center for Therapeutic Oncology Research, UT Southwestern Medical Center, Dallas, TX, USA. ²Department of Pharmacology, UT Southwestern Medical Center, Dallas, TX, USA. ³Department of Internal Medicine, UT Southwestern Medical Center, Dallas, TX, USA. ⁴Simmons Comprehensive Cancer Center, UT Southwestern Medical Center, Dallas, TX, USA. ⁵Department of Surgery, UT Southwestern Medical Center, Dallas, TX, USA. ✉email: elisabeth.martinez@utsouthwestern.edu

Received: 10 January 2024 Revised: 30 July 2024 Accepted: 6 August 2024

Published online: 18 August 2024

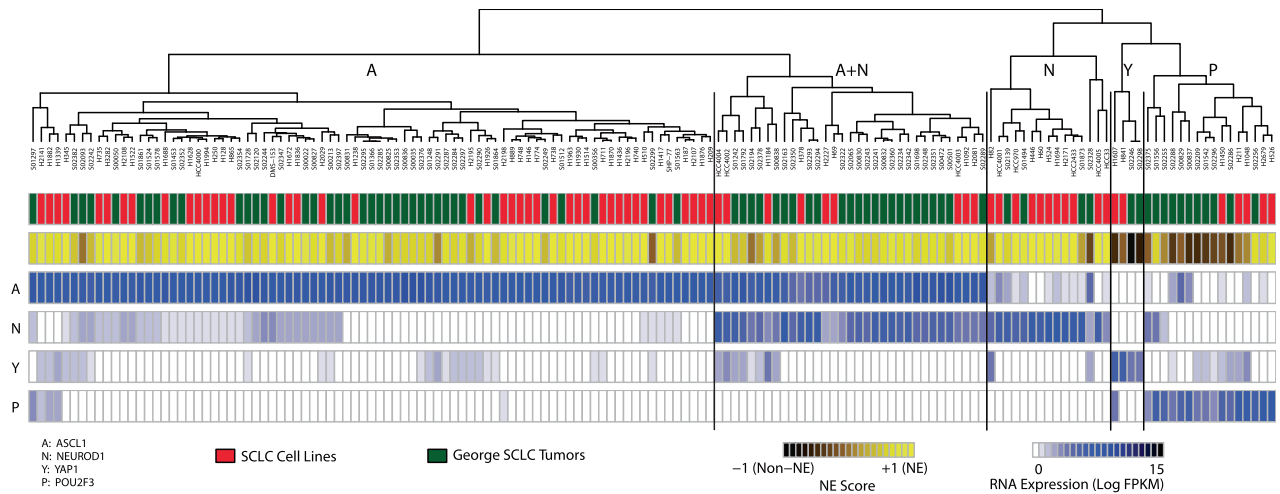


Fig. 1 Clusters of SCLC cell lines and patient tumors driven by lineage transcription factors. Cell lines are shown in red and patient tumors are shown in green in the top bar. Neuroendocrine score, defined by the level of expression of 50 genes that drive the neuroendocrine phenotype [27], is represented on a yellow-to-brown scale. Relative transcription factor expression levels are shown in blue scale and are defined as follows: *ASCL1* – A, *NEUROD1* – N, *YAP1* –Y, and *POU2F3* – P. Note that cell lines populate all the clusters defined in patient samples.

repression of NOTCH signaling [24]. In the present study, we evaluate the effects of pharmacological and genetic ablation of Jumonji demethylase activity on the growth and molecular features of SCLC. We report that pharmacologic inhibition of Jumonji KDM activity and genetic downregulation of KDM4A in SCLC activates the endoplasmic reticulum (ER) stress signaling pathway and mTOR signaling genes, and decreases expression of SCLC NE markers and oncogenic proteins including lineage transcription factors. Importantly, these Jumonji inhibitor mechanisms of action are also at play in vivo leading to blunted growth of SCLC tumor xenografts representing *ASCL1*⁺, *NEUROD1*⁺, and etoposide-resistant disease. Our preclinical findings point toward a new treatment strategy to abrogate SCLC tumor growth through blocking KDM activity in vivo and uncover a new mechanism of action of Jumonji inhibitors through the activation of ER stress and downregulation of SCLC-promoting proteins.

RESULTS

Jumonji inhibitors curtail the viability of SCLC cell lines across transcription factor subtypes

To determine if SCLC lines in culture reflected expression patterns similar to patient specimens, we performed hierarchical clustering using the gene expression levels of the four lineage transcription factor genes across our own 78 patient-derived SCLC cell lines and 87 patient-derived tumor specimens from published datasets [25, 26]. We identified five unique clusters, characterized by the dominant transcription factor(s) expression in each group *ASCL1* – A, *NEUROD1* – N, *POU2F3* – P, and *YAP1* –Y, plus a fifth group representing the A + N co-expressing cluster (Fig. 1). This is in agreement with previous findings reported by the NCI group, whose dataset contained 19 distinct and 35 overlapping SCLC lines compared to our analysis [12]. Notably, both the SCLC lines and the tumor specimens had near equivalent representations in any one cluster, demonstrating that SCLC cell lines investigated in this study are a biologically consistent representation of transcriptomic expression profiles found in patient tumors. We also used a 50-gene expression-based neuroendocrine (NE) scoring system [27] to quantify the neuroendocrine properties of the cell lines and tumors. As expected, the *POU2F3* and *YAP1* groups generally express lower NE scores compared to other clusters.

With these preclinical SCLC models in hand, we first analyzed the expression levels of the major members of the oncogenic

Jumonji lysine demethylase family by RNA-seq. As seen in Fig. S1A, these genes were widely expressed in the 78 SCLC lines compared to the 21 human bronchial epithelial cells evaluated, with members of the KDM4 and KDM5 family being among the highest expression (see also Supplementary RNA-seq dataset, tab for Fig. S1A). Western immunoblot analysis confirmed this at the protein level (Fig. S1B), encouraging us to study their potential as SCLC therapeutic targets.

We evaluated a panel of ~30 SCLC lines representing the four largest transcription factor clusters (A, A + N, N, P) against JIB-04 (a pan-Jumonji inhibitor developed by our group), SD70 (KDM4 sub-family inhibitor), as well as GSK-J4 (KDM6 sub-family inhibitor) and measured viability after 4-day drug exposure via MTS viability assays. We found that the viability of SCLC lines is significantly decreased by the Jumonji inhibitors, with JIB-04 being the most potent (Table 1 and Fig. 2A). SCLC lines showed a wider range of sensitivities to JIB-04 and GSK-J4 than to SD70 with SD70 being moderately more potent, on average, than GSK-J4 (Fig. 2A). Among the three Jumonji inhibitors, the correlation coefficients between the IC_{50} s of JIB-04 and SD70 and between JIB-04 and GSK-J4 were strongly positive across the SCLC panel, as expected by their overlapping specificities, while much weaker between GSK-J4 and SD70 (Fig. S1C). To investigate on-target activity by these small molecule inhibitors, we selected SCLC line NCI-H446 (H446) which was highly sensitive to JIB-04, and NCI-H2171 (H2171) cells, which showed lower responsiveness, and measured actual Jumonji demethylase activity in lysates from cells treated with IC_{50} doses for 24 h. Demethylase activity on an exogenous H3K9me3 substrate was quantified by ELISA to detect the demethylated H3K9me2 product as previously described [28–32]. In line with viability assays, we found that H446 (left panel) and H2171 (right panel) Jumonji demethylase activities were inhibited by JIB-04 and by SD70 treatment compared to DMSO in lysates from cells treated with the corresponding IC_{50} doses (Fig. 2B). This confirmed on-target inhibition of Jumonji demethylases in SCLC by these agents, both of which blocked the generation of H3K9me2 from H3K9me3 substrates.

Etoposide-resistant SCLC cell lines are among the most sensitive to Jumonji inhibitors

To compare the sensitivity profiles of SCLC to Jumonji inhibitors vs standard-of-care etoposide, we also determined the response phenotypes to etoposide across our SCLC line panel (Table 1). Polley et al. reported the response to etoposide of a number of

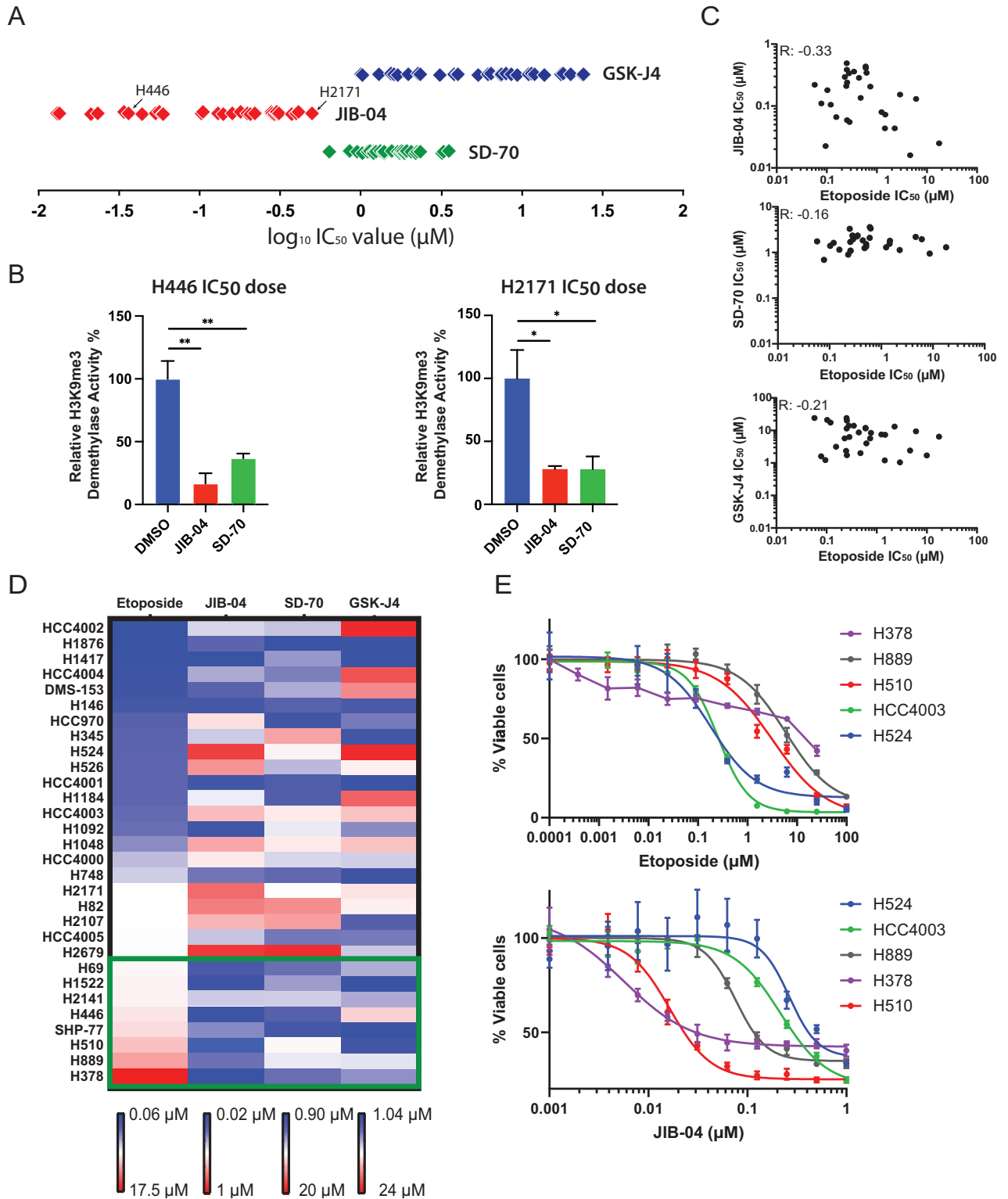
Table 1. IC₅₀ values of etoposide, JIB-04, SD70, and GSK-J4 across 31 SCLC cell lines representing all transcription factor subgroups.

Cell Line	Etoposide (μM)			JIB-04 (μM)			SD70 (μM)			GSK-J4 (μM)		
	Assays	IC ₅₀	SD	Assays	IC ₅₀	SD	Assays	IC ₅₀	SD	Assays	IC ₅₀	SD
DMS-153	3	0.12	0.02	2	0.105		2	1.9		2	17.5	
H1048	6	0.36	0.07	7	0.29	0.093	6	2.35	2.2	4	6.15	8.1
H1092	4	0.26	0.05	2	0.055		2	1.95		2	6.3	
H1184	2	0.26		3	0.14	0.15	2	1.08		1	18	
H1417	2	0.1		10	0.0225	0.17	3	1.4	0.23	3	1	0.41
H146	15	0.1	0.12	8	0.0665	0.44	2	1.15		2	3.15	
H1522	2	1.45		3	0.056	0.78	2	1.55		3	1.3	0.37
H1876	2	0.08		2	0.106		2	0.685		2	1.55	
H2107	8	0.71	0.22	3	0.3	0.084	2	3.35		2	4	
H2141	5	1.5	0.34	2	0.195		2	1.8		2	7.35	
H2171	18	0.59	0.23	10	0.495	0.29	2	2.1		2	12	
H2679	2	0.56		1	>1		1	>20		2	8.4	
H345	2	0.25		2	0.21		2	3.3		2	2.35	
H378	2	17.5		2	0.024		3	1.2	0.26	2	6.45	
H446	3	2	0.55	8	0.034	0.019	7	1.2	0.54	5	7.4	6
H510	4	4.45	1.64	5	0.021	0.014	2	2.2		2	2.35	
H524	7	0.29	0.15	6	0.41	0.21	2	2.25		3	24	5.8
H526	13	0.23	0.1	3	0.28	0.16	2	1.7		2	11.4	
H69	18	0.88	0.82	8	0.082	0.51	3	1.4	0.17	2	7.5	
H748	2	0.48		3	0.13	0.05	2	1.25		2	2	
H82	21	0.58	0.32	2	0.41		2	3.6		2	11.5	
H841	3	9.4	3.78	2	0.38		2	1.85		2	1.7	
H889	13	5.7	1.41	3	0.13	0.01	2	1.95		2	9.35	
HCC4000	2	0.44		2	0.285		2	1.85		2	8.65	
HCC4001	2	0.26		4	0.059	0.036	3	1.1	0.23	3	1.6	0.42
HCC4002	4	0.1	0.04	2	0.22		2	1.75		2	24	
HCC4003	3	0.28	0.02	3	0.31	0.064	2	2.35		2	14	
HCC4004	2	0.1		2	0.18		2	1.4		2	21	
HCC4005	2	0.74		2	0.205		2	1.35		2	4	
HCC970	2	0.23		3	0.3	0.38	2	0.9		2	5.7	
SHP-77	2	1.44		3	0.16	0.021	2	0.945		2	1.04	

Cells were treated with drugs for 4 days, then cell viability was measured by MTS assay. Shown are median values with standard deviations ($n = 2-21$).

SCLC lines and compared them to their response to several hundred other therapeutics or pipeline drugs and found strong positive correlations of all tested agents with etoposide response, highlighting SCLC as a recalcitrant disease [14]. To confirm that we had similar etoposide response phenotypes to those reported by Polley et al. we compared our data to that reported by the NCI group and found the relative IC₅₀ values to be well correlated across the two studies for common cell lines included in both panels (Fig. S2A). Given that SCLC lines had responses to multiple drug categories similar to the response to etoposide in the Polley dataset [14], we analyzed the correlation between etoposide IC₅₀ and Jumonji inhibitor IC₅₀ across our SCLC panel, since Jumonji inhibitors were not evaluated by Polley et al. Importantly, these were not positively correlated: the etoposide-JIB-04 IC₅₀ correlation coefficient was -0.33 , the etoposide-SD70 IC₅₀ correlation coefficient was -0.16 , and the etoposide-GSK-J4 IC₅₀ correlation coefficient was -0.21 (Fig. 2C). Thus, all three Jumonji inhibitors showed patterns anti-correlated with the SCLC response phenotypes to etoposide, indicating the possibility that Jumonji targeting drugs may be effective against etoposide-resistant SCLC. Indeed, when we analyzed the sensitivities of SCLC to

these inhibitors ranking them by etoposide IC₅₀, (Eto_S for IC₅₀ < 0.3 μM, Eto_M for IC₅₀ < 0.8 μM and > 0.3 μM or Eto_R for IC₅₀ > 0.8 μM) it became clear that the eight cell lines that are more resistant to etoposide are generally highly sensitive to Jumonji inhibitors and to JIB-04 in particular (Fig. 2D, as highlighted in the green box). In fact, the three SCLC lines most resistant to etoposide, H510(A⁺, Eto_R), H378(A + N⁺, Eto_R), and H889(A⁺, Eto_R) are among the most sensitive to JIB-04 (Fig. 2E). Similarly, SD70 was highly effective against H446 (N⁺, Eto_R), H378 (A + N⁺, Eto_R) and SHP-77 (A⁺, Eto_R), lines which are resistant to etoposide (Fig. S2B). When we analyzed the transcription factor SCLC clusters, we observed that, in general, each cluster harbored both Jumonji demethylase inhibitor sensitive and less sensitive lines with the NEUROD1-high group showing the widest range of response (Fig. S2C, D) and the POU2F3 cluster being less sensitive to Jumonji inhibition (Fig. S2C). Further analysis uncovered that JIB-04 is on average more potent against ASCL1-high cell lines vs NEUROD1-high lines (Fig. S2E) and against cell lines with high NE score (Fig. S2F), suggesting that at least in these subtypes JIB-04 may block multiple KDM targets. Thus, responsiveness to Jumonji inhibition was generally found in all of the lineage transcription



factor subgroups. Importantly, response to all Jumonji inhibitors tested was not correlated with response to etoposide, a unique feature compared to all the drug categories tested by Polley et al.

Jumonji inhibitors sensitize a subset of SCLC to mTOR inhibition and widely induce ER stress response genes

To determine which potential mechanisms may be involved in or pathways activated by Jumonji inhibitors in SCLC, we performed

bulk RNA-seq analysis on control vs. treated cells. Gene set enrichment analysis of RNA-seq data uncovered, for example, that a subset of SCLC cell lines (ie, H2171-N⁺, Eto_M, H524-N⁺, Eto_S) upregulated genes in the mTOR signaling pathway (Fig. 3A and Supplementary RNA-seq dataset file, tab for Fig. 3A). We, therefore, hypothesized that Jumonji inhibition may sensitize these cells to mTOR inhibitors, which are used clinically. We found that H2171(N⁺, Eto_M) and H524 (N⁺, Eto_S) were indeed

Fig. 2 **Jumonji inhibitors block SCLC viability, act on target, and robustly inhibit etoposide-resistant cell lines.** **A** Range of IC_{50} responses to JIB-04, SD70, and GSK-J4 of SCLC cell lines representing all clusters. Each diamond represents the median IC_{50} across multiple experiments of a particular cell line, measured by 4-day MTS assay (see also Table 1). The IC_{50} values are shown on a log scale. **B** Inhibitors act on target as demonstrated by robust decreases in Jumonji enzymatic activity when cells are treated with their corresponding IC_{50} values for 24 h. Bar graphs display the level of H3K9me3 demethylase activity in H446 and H2171 cell lysates and/or nuclear extracts after the indicated treatment. ** = $p \leq 0.01$ and * = $p \leq 0.05$ by two-tailed *t*-test, unequal variance. Data are average \pm SEM. **C** Correlation analysis yields negative correlations between the IC_{50} of etoposide and the IC_{50} of each of the three Jumonji inhibitors tested across 31 SCLC cell lines: JIB-04 (pan-JmjC KDM inhibitor with some selectivity for KDM5s), SD70 (relatively selective KDM4 inhibitor) and GSK-J4 (relatively selective KDM6 inhibitor). Pearson *R*-values are shown. **D** Heat map of etoposide and Jumonji inhibitor IC_{50} values represented in a blue to red scale for individual drugs in the indicated concentration ranges. Chemoresistant cell lines in the green box are sensitive to Jumonji inhibitors, particularly to JIB-04. **E** Dose-response curves demonstrate three etoposide most resistant cell lines (H378, H889, and H510) are highly sensitive to JIB-04. H524 and HCC4003 are sensitive to etoposide and are given for reference. Representative curves of $n = 4-8$ replicates with SEM are shown. See Table 1 for further details.

sensitized to mTOR inhibitors when co-treated with constant low concentrations of JIB-04 (respective IC_{25}) (Fig. 3B). On the other hand, HCC4001(N⁺, Eto_S) which did not significantly upregulate the mTOR pathway in response to Jumonji inhibition (Fig. S3A), did not show hypersensitivity to mTOR inhibitors when treated with IC_{25} JIB-04 (Fig. 3C).

RNA-Seq analysis also revealed that among gene sets commonly enriched across multiple SCLC lines (Fig. S3B), the ER stress pathway scored consistently high, and multiple genes in the ER stress response including *ATF4*, *ATF3*, *DDIT3*, *FGF21*, *CHAC1*, *INHBE* and *VLDLR* were significantly upregulated across many SCLC lines regardless of transcription factor subtype or etoposide sensitivity H510(A⁺, Eto_R), HCC4001(N⁺, Eto_S), H2171(N⁺, Eto_M), H524 (N⁺, Eto_S) (Fig. S3C, D). We next examined if ER stress gene activation had functional consequences at the protein level.

ER stress proteins are elevated and cell death is triggered in SCLC treated with Jumonji inhibitors

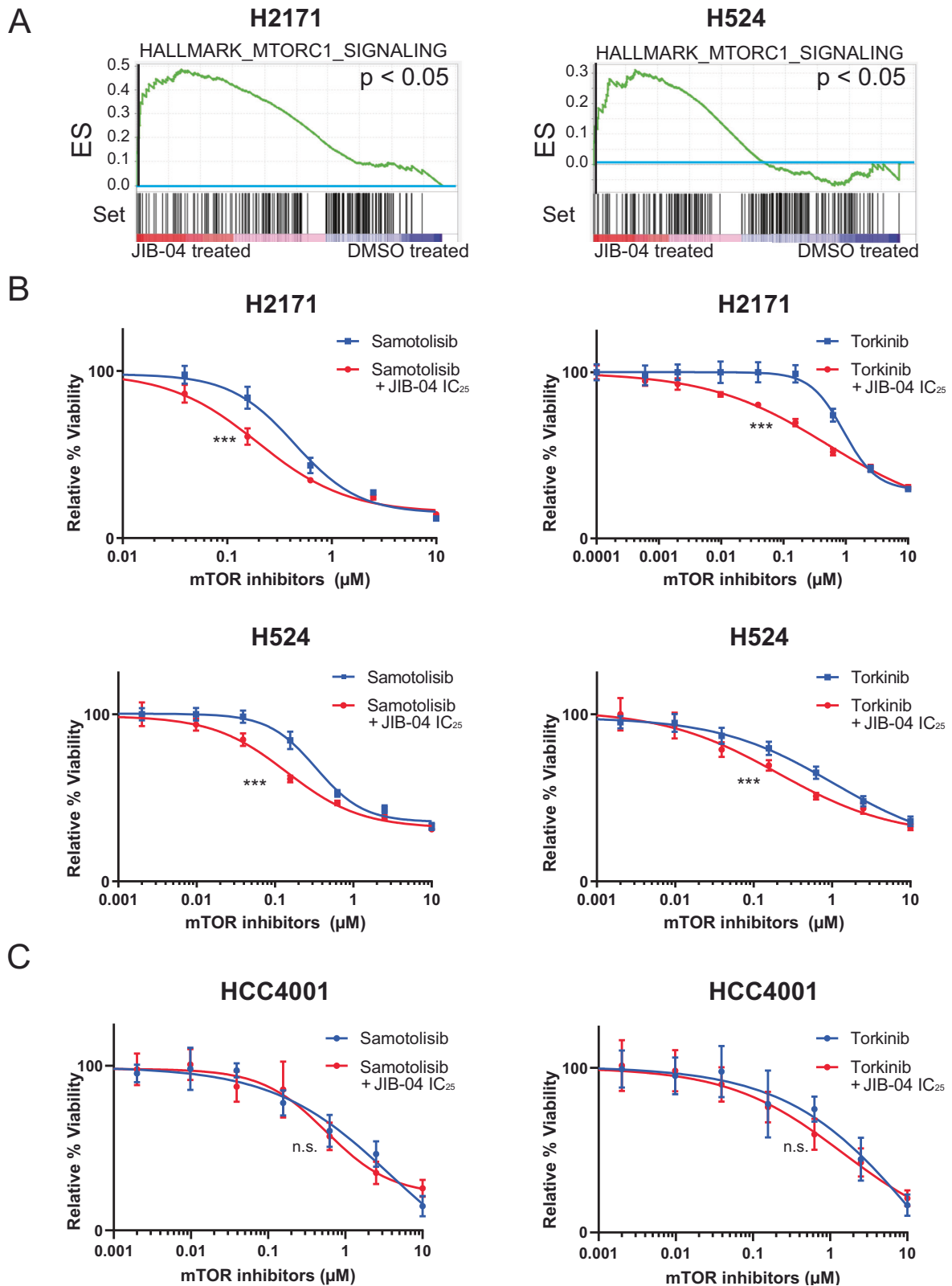
To evaluate if the upregulation of ER stress gene expression in response to JIB-04 was seen also at the protein level and with other inhibitors of Jumonji enzymes, we performed Western blot analysis on lysates of a wide range of SCLC cells representing both ASCL1-high as well as NEUROD1-high disease. Cells were treated with JIB-04 or SD70 for 24 h and probed for multiple proteins involved in ER stress. ATF4 protein expression was robustly upregulated by both JIB-04 and SD70 treatment (similarly to that recently reported by GSK-J4) across multiple SCLC lines as was its downstream target, DDIT3 (Fig. 4A and quantification in Fig. S4A) [33]. ATF3 protein expression, another ATF4 target [34], was likewise upregulated (Fig. S4B). Furthermore, a subset of SCLC lines also showed activation of phospho-eIF2 α at this time point (Fig. 4B and quantification in Fig. S4C), indicating functional activation of the ER stress response [35]. The upregulation of these ER stress proteins was commonly seen in both ASCL1-high (H510-Eto_R, H1522-Eto_R, H1417-Eto_S, H2107-Eto_M) and in NEUROD1-high lines (H446-Eto_R, H524-Eto_S, H2171-Eto_M) and in cells across the full range of etoposide IC_{50} s, in response to Jumonji inhibitors. Upregulation of ER stress was followed by the onset of apoptosis/cell death in the full range of SCLC cells as measured by Annexin V staining and PARP cleavage (Fig. 4C, D).

Depletion of the transcriptional regulator Jumonji KDM4A upregulates ER stress genes and mTOR signaling genes in SCLC cells, decreases cell proliferation in vitro, and blunts tumor growth in vivo

Our initial quantification of Jumonji demethylase gene expression and protein levels across SCLC lines indicated that KDM4A and KDM5B were the Jumonji enzymes most highly and widely expressed in this cancer (Fig. S1A and Supplementary RNA-seq dataset, tab for Fig. S1A). In DepMap neither KDM4A nor KDM5B scored as pan-essential genes. Together, these facts suggest that KDM4A and/or KDM5B may be relevant contributors to SCLC oncophenotypes. We therefore used CRISPR/Cas technology to

downregulate the expression of each of these two Jumonji enzymes in H446(N⁺, Eto_R) cells which had shown high levels of both of these proteins by Western blot (Fig. S1B). We obtained knockdown of KDM4A (Fig. 5A) and KDM5B (Fig. S5A, left panel). In the KDM4A knockdown H446(N⁺, Eto_R) cells we observed 50% growth inhibition compared to the two control cell lines (parental and Cas9-only) at day 17 of continuous proliferation (Fig. 5B). By contrast, KDM5B knockdown cells did not show a growth suppression phenotype under identical conditions (Fig. S5A, right panel). In agreement with the anti-proliferative effect of KDM4A downregulation, another recently developed more potent inhibitor of the KDM4 family, TACH101 [36], robustly blocked the demethylase activity of purified KDM4A (Fig. S5B, top panel) and potently inhibited SCLC cell viability (Fig. S5B, bottom panel). Taking together these results, and with the fact that there is evidence for KDM4A regulation of a subset of ER stress genes [37–42] which we confirmed by bioinformatics analysis (Fig. S5C Venn diagram and Supplementary RNA-seq dataset tab for Fig. S5C), we hypothesized that KDM4A may be partly driving SCLC growth and partly mediating Jumonji inhibitor phenotypes. Consistent with this notion, we found that KDM4A knockdown H446 cells also formed 40% fewer colonies compared to the two control cell types (Fig. 5C). Furthermore, multiple ER stress pathway genes were upregulated by at least 50% in the KDM4A knockdown H446 cells compared to the parental and the Cas9-only controls (Fig. 5D and longer list in Supplementary RNA-seq dataset, tab for Fig. 5D). This phenotype mimicked aspects of our findings with pharmacologic inhibition of Jumonji KDM activity in treated cells where we saw decreased activity of H3K9me3 demethylases (i.e., the KDM4 subfamily) and the induction of ER stress genes (Fig. 2B and Fig. S3B). p-eIF2 α was also activated and several other ER stress proteins were also upregulated in the KDM4A knockdown cells (Fig. 5E, quantification in Fig. S5C right panels). Furthermore, we observed that the KDM4A knockdown H446 cells showed highly significant upregulation of mTOR signaling genes (Fig. S5D, right panel) and were also sensitized to mTOR inhibitors (Fig. 5F), as we had seen earlier with Jumonji inhibitor treatment (Fig. 3 and Fig. S5D, left panel). These results all point to KDM4A genetic or functional blockade as a component of the Jumonji inhibitor-mediated anti-growth effects on SCLC, across subtypes.

To determine if the growth phenotypes observed in vitro were recapitulated in vivo, equal numbers of parental H446(N⁺, Eto_R) cells, H446 with constitutive Cas9 expression, or H446 KDM4A knockdown cells were injected subcutaneously into the right flanks of athymic nude mice. After 25 days, all mice were sacrificed and subcutaneous tumors were resected. H446 KDM4A knockdown tumors retained the loss of KDM4A as confirmed by Western blot (Fig. S5E). Importantly, KDM4A loss inhibited the growth of the H446(N⁺, Eto_R) tumors compared to the two control groups (Fig. 5G, H). Final tumor weights also decreased with loss of KDM4A compared to controls (Fig. S5F–I). To confirm the generality of our findings, we next genetically depleted KDM4A



in a second NEUROD1-high cell line (H524) as well as in an ASCL1-high cell line (H1522). As shown in Fig. S5J, depletion of KDM4A resulted in blunted proliferation over multiple time points, indicating this Jumonji enzyme affects growth across the two main SCLC subtypes.

Jumonji KDM pharmacological inhibition blocks tumor growth in vivo and alters the expression of KDM regulated genes

We next evaluated the in vivo efficacy of Jumonji inhibitors JIB-04 and SD70, against H446(N⁺, Eto_R) parental cell xenografts. Tumor cells were injected subcutaneously, and tumors allowed to grow

Fig. 3 A subset of SCLC lines upregulates mTOR signaling genes and is sensitized to mTOR inhibitors in response to JIB-04 treatment. **A** SCLC cell lines (H2171 and H524) upregulated mTOR signaling pathway genes upon treatment with JIB-04 at 0.05 μM as determined by GSEA analysis. Nominal p-values are shown as calculated on the GSEA site following Subramanian et al. [61]. See Supplementary Information RNA-seq dataset for more details. **B** Dose-response curves to each of two different mTOR inhibitors alone and concurrently with low dose of JIB-04 (IC_{25}) measured by MTS viability assays over a 4-day treatment. The two cell lines that upregulated mTOR signaling genes in response to JIB-04 have 2–3-fold or greater enhanced sensitivity to mTOR inhibitors (mean \pm SEM is shown for each dose, $n = 3\text{--}4$). **C** HCC4001 which did not significantly upregulate mTOR signaling genes in response to JIB-04, did not show enhanced sensitivity to mTOR inhibitors (mean \pm SD is shown for each dose, $n = 8$). **B, C** JIB-04 $\text{IC}_{25} = 0.25 \mu\text{M}$ for H2171 and H524, $0.01 \mu\text{M}$ for HCC4001. P-values for curve comparisons calculated by GraphPad Prism (top, bottom, IC_{50} , Hill coefficient) are as follows: H2171 Samotolisib \pm JIB-04 0.0069; H2171 Torkinib \pm JIB-04 < 0.0001 , H524 Samotolisib \pm JIB-04 0.0005, H524 Torkinib \pm JIB-04 0.0011, HCC4001 Samotolisib \pm JIB-04 0.1425, HCC4001 Torkinib \pm JIB-04 0.1932.

to $\sim 150\text{--}200 \text{ mm}^3$. Once tumors were established, animals with similar tumor volumes were paired to receive vehicle or Jumonji inhibitor treatment as described in the Materials and Methods. H446 tumors treated with JIB-04 exhibited $\sim 75\%$ less growth compared to vehicle-treated controls with tumor volumes being significantly smaller with JIB-04 treatment (Fig. 6A, left panel). Final tumor weights were also significantly reduced in the treatment cohort (Fig. 6A, right panel). SD70 treatment of H446(N^+ , Eto_R) xenografts led to a $\sim 50\%$ significantly reduced tumor volume (Fig. 6B, left panel) and lower final tumor weights (Fig. 6B, right panel). We validated these findings in a second model by testing the efficacy of the more KDM4-specific inhibitor SD70 against H510(A^+ , Eto_R) xenografts in vivo, where treatment caused a $\sim 60\%$ reduction in tumor volumes and significantly lower tumor weights in the SD70-treated mice (Fig. 6C). Neither JIB-04 nor SD70 caused any overt toxicities in the mice, and the animals maintained their body weights throughout the treatment period (Fig. S6A). To understand the molecular changes that may accompany the anti-growth phenotypes triggered by Jumonji inhibitor treatment in vivo, we performed bulk RNA-seq on residual tumor samples harvested when the mice were sacrificed. Alignment of differentially expressed genes in JIB-04/vehicle or in SD70/vehicle-treated tumors with KDM4A target genes (Supplementary RNA-seq dataset, tab for Fig. S6B left panel), yielded an overlap of 20–25% for all comparisons (Fig. S6B). Thus, about a fifth to a fourth of the genes altered in vivo by JIB-04 or SD70 treatment in H446(N^+ , Eto_R) or H510(A^+ , Eto_R) xenografts correspond to genes that are KDM4A target genes (Fig. S6B) including ER stress genes (Supplementary RNA-seq dataset, tab for Fig. S6B middle panel). In addition, we observed a 35% overlap between genes upregulated by JIB-04 and SD70 in H446 xenografts, indicating partial common in vivo targets of these two compounds (Fig. 6D left panel and Supplementary RNA-seq dataset, tab for Fig. 6D left panel). Furthermore, there was a 34% overlap between genes upregulated by SD70 in H446(N^+ , Eto_R) xenografts and genes upregulated by SD70 in H510(A^+ , Eto_R) xenografts (Fig. 6D right panel and Supplementary RNA-seq dataset, tab for Fig. 6D right panel), indicating both common and distinct targets in NEUROD1 (H446- Eto_R) vs ASCL1-high (H510- Eto_R) xenografts and confirming Jumonji inhibitor efficacy in vivo against two models of etoposide-resistant disease.

Both Jumonji KDM inhibition and KDM4A knockdown alter the levels of key modulators of SCLC phenotypes

To understand what proteins may be affected by Jumonji inhibitors contributing to the observed growth phenotypes, we utilized mass spectrometry to analyze H446(N^+ , Eto_R) lysates derived from parental cells treated with vehicle, JIB-04 or SD70 (IC_{50} , 24 h) along with lysates of the H446 Cas9 and H446 KDM4A knockdown genetic pair. Among the proteins that were commonly downregulated by JIB-04 treatment, SD70 treatment, and KDM4A knockdown was the SCLC marker Secretogranin-3 [43–45] (Supplementary Table 3). We confirmed the downregulation of this SCLC marker in the culture media of the H446 KDM4A knockdown cells by Western blot (Fig. 7A and Fig. S7A). Remarkably, among the proteins that were commonly

downregulated by JIB-04, SD70, and KDM4A knockdown was also INSM1 (Supplementary Table 3), a marker of neuroendocrine differentiation in SCLC that modulates lineage transcription factors [46–48]. We therefore probed H446 KDM4A knockdown cell lysates by Western blot and confirmed INSM1 protein downregulation in the KDM4A-depleted H446 cells while the H446 KDM5B-depleted cells did not alter INSM1 protein levels (Fig. 7B, Fig. S7B). INSM1 protein was also downregulated in Jumonji inhibitor-treated NEUROD1-high and ASCL1-high cells vs controls (Fig. 7B, Fig. S7B), indicating a general effect across these SCLC subtypes and including etoposide-resistant cells. Furthermore, the downregulation of INSM1 was concomitant with decreased levels of driver transcription factors NEUROD1 (H446(N^+ , Eto_R), HCC4001(N^+ , Eto_S)) or ASCL1 protein (H510(A^+ , Eto_R), H2107(A^+ , Eto_M)) as measured by Western blot analysis in the respective cell line subtypes (Fig. 7C, Fig. S7C). To evaluate if these changes were also occurring in vivo, we analyzed nuclear extracts from two available pairs of H510 tumors treated with SD70 vs vehicle. Consistent with on-target action of SD70, we found H3K9me3 levels elevated by Western blots (Fig. 7D). This was accompanied by downregulation of both INSM1 and ASCL1 protein levels (Fig. 7E). In line with the downregulation of ASCL1, we also observed upregulation of NOTCH signaling genes by RNA-seq in H510(A^+ , Eto_R) tumor xenografts treated with SD70 in vivo (Supplementary I RNA-seq dataset, Fig. 7 NOTCH tab). Taken together, these results suggest that pharmacological Jumonji enzyme inhibition or KDM4A genetic downregulation across the main subtypes of SCLC trigger decreased SCLC growth in part by activating ER stress, and downregulating key players of SCLC including INSM1, ASCL1 or NEUROD1 and Secretogranin-3, leading to apoptosis.

DISCUSSION

Here we have established the efficacy of multiple Jumonji demethylase inhibitors against the growth of SCLC lines and of JIB-04 and SD70 against xenograft tumors representing ASCL1-high and NEUROD1-high subtypes. Our results indicate that the anti-proliferative action of these inhibitors is potent even against etoposide-resistant disease and involves activation of ER stress [49] and protein downregulation of key markers and oncogenic drivers of the SCLC phenotype, including the Secretogranin-3 chromogranin protein, the INSM1 transcriptional repressor, and the lineage transcription factors ASCL1 and NEUROD1. This intriguing mechanism of action of Jumonji inhibitors in the context of SCLC was partly mimicked in cells and in vivo by the genetic knockdown of KDM4A, a Jumonji enzyme highly and widely expressed in SCLCs and a common target of JIB-04 and SD70. Interestingly, although the pan-inhibitor JIB-04 was significantly more potent, on average, against ASCL1-high SCLC, the other inhibitors, including the KDM4 selective SD70, did not show any subtype preference. KDM4A may thus represent a common target across the main subtypes of SCLC. In line with this, TACH101, another potent inhibitor of the KDM4 family, confirmed robust blockade of SCLC viability across subtypes including etoposide-resistant cells. Although KDM4A genetic knockdown mimicked multiple Jumonji inhibitor phenotypes, the action of JIB-

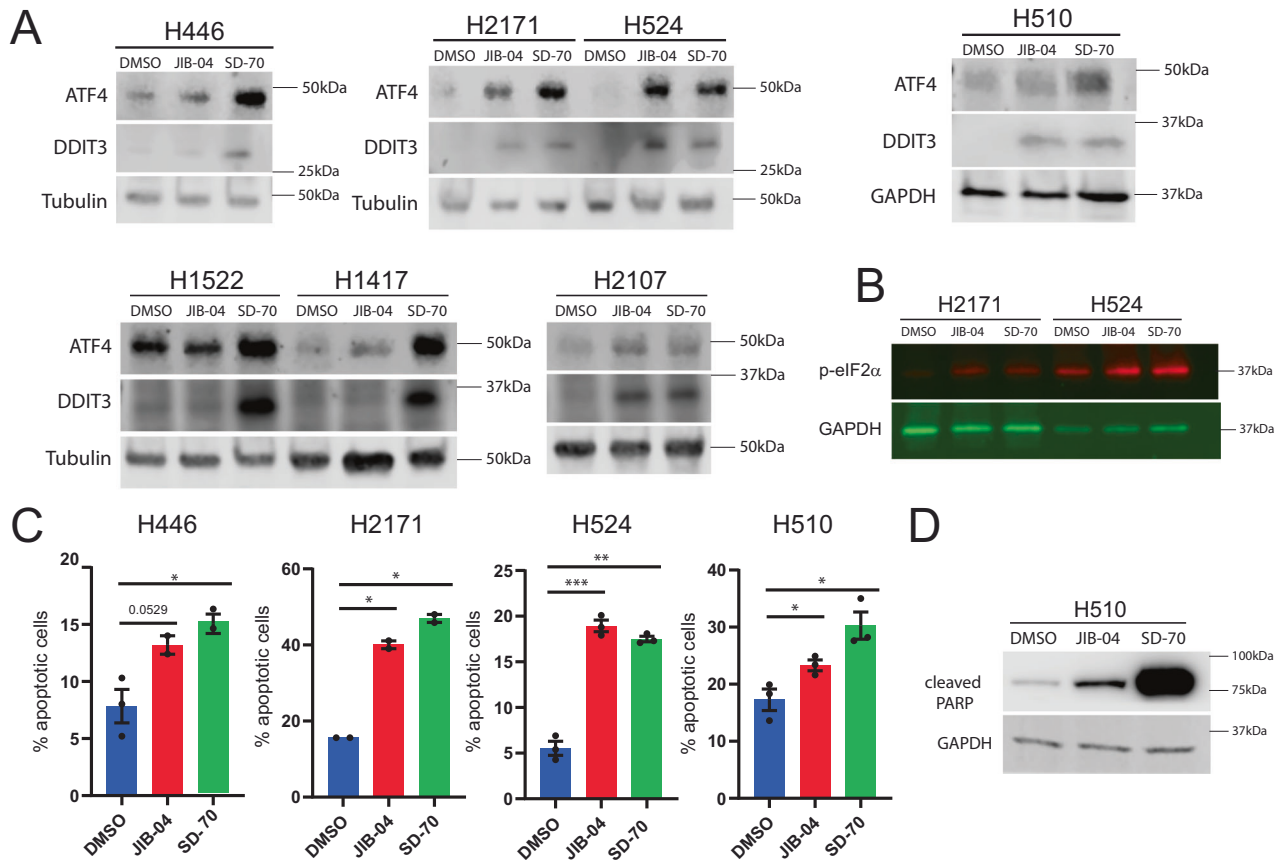


Fig. 4 Jumonji inhibitors activate ER stress pathway proteins and trigger cell death in SCLC cells. **A** Western blot analysis demonstrates multiple proteins in the ER stress pathway are elevated by treatment with IC₅₀ doses of JIB-04 or SD70 for 24 h across multiple SCLC lines representing various inhibitor sensitivities and both NEUROD1-high (H446, H2171, H524) and ASCL1-high transcription (H510, H1522, H1417, H2107) factor clusters. Tubulin or GAPDH were used as a loading control. **B** Activation of phospho-eIF2α is also seen by Western analysis in SCLC cell lines treated with inhibitors for 24 h at their respective IC₅₀. GAPDH was used as loading control. **C** Annexin V staining was analyzed by FACS after 48 h (H446, H2171, H510) or 72 h (H524) of inhibitor treatment, and double-positive early or late apoptotic cells quantified. Data are averages across replicates with error bars representing SEM. **** = $p \leq 0.0001$, *** = $p \leq 0.001$, ** = $p \leq 0.01$, * = $p < 0.05$, by unpaired two-tailed *t*-test. **D** Inhibitor treatment with IC₅₀ for 48 h triggers PARP cleavage in H510 as shown by Western blot, indicating late stage of apoptosis. GAPDH served as a loading control. **C** shows quantification of early apoptotic H510 cells at this time point.

04 or SD70 may also be partly mediated by other Jumonji enzymes in SCLC.

While knockdown of highly expressed Jumonji KDM5B did not alter INSM1 levels nor had an effect on growth, downregulation of its sister protein KDM5A has been shown by the Kaelin group to affect ASCL1-driven SCLC growth in vivo. The oncogenic roles of KDM5A in the context of Rb1 null cancers has been recently recognized [24, 50, 51] and involves negative regulation of NOTCH signaling genes. RNA-seq data of H510(A⁺, Eto_R) residual tumors treated with SD70 in our study indicated multiple genes in the NOTCH signaling pathway are upregulated in vivo by Jumonji KDM4 inhibitor treatment, notably including a three-fold upregulation of JAG2 ligand, and two-fold upregulation of HES1 and SPEN transcription factors, all of which can modulate ASCL1 action [24, 52, 53]. In addition, downregulation of ASCL1 protein itself was seen by us in H510 cells as well as in other ASCL1-high lines treated with Jumonji inhibitors indicating a potential common mechanism to which multiple KDMs may contribute to decrease ASCL1 function. Indeed, we confirmed this downregulation of ASCL1 by SD70 in vivo. The action of Jumonji inhibitors or KDM4A knockdown in downregulating the protein levels of INSM1, ASCL1 or NEUROD1 would predict that SCLC with low neuroendocrine properties would be less responsive to these interventions. This is indeed the case with the POU2F3 subtype which we found to

be less sensitive to Jumonji inhibitors compared to the other TF subtypes.

Several lines of evidence suggest overlapping mechanisms of action of JIB-04 and SD70. First, these two compounds show a strong positive correlation in terms their relative IC₅₀ values across ~30 SCLC lines tested, showing parallel sensitivities. Secondly, they both markedly decrease the activity of Jumonji KDM4 H3K9me3 demethylases in small cell lung cancer cells. In addition, they have overlapping profiles in vivo. For example, they share 35% gene targets. Interestingly, among the genes commonly upregulated by JIB-04 and SD70 and by SD70 in both H446(N⁺, Eto_R) and H510(A⁺, Eto_R) xenograft models, we found >20 genes that are downregulated by ZFP91. This may be mechanistically important since ZFP91 is known to have oncogenic functions in multiple tumor types [54–56] and thus Jumonji inhibitors may be reversing a subset of these tumor-promoting properties.

In conclusion, our studies have identified a novel therapeutic strategy using Jumonji inhibitors to target SCLCs including etoposide-resistant disease, and a potential common target across SCLC subtypes, KDM4A. We have also uncovered a new mechanism for the anti-cancer action of Jumonji inhibitors in SCLC that includes the activation of ER stress and the downregulation of expression of proteins known to drive aspects of SCLC including Secretogranin-3, INSM1, ASCL1, and NEUROD1. With the advent of clinical trials for this drug class with the KDM4

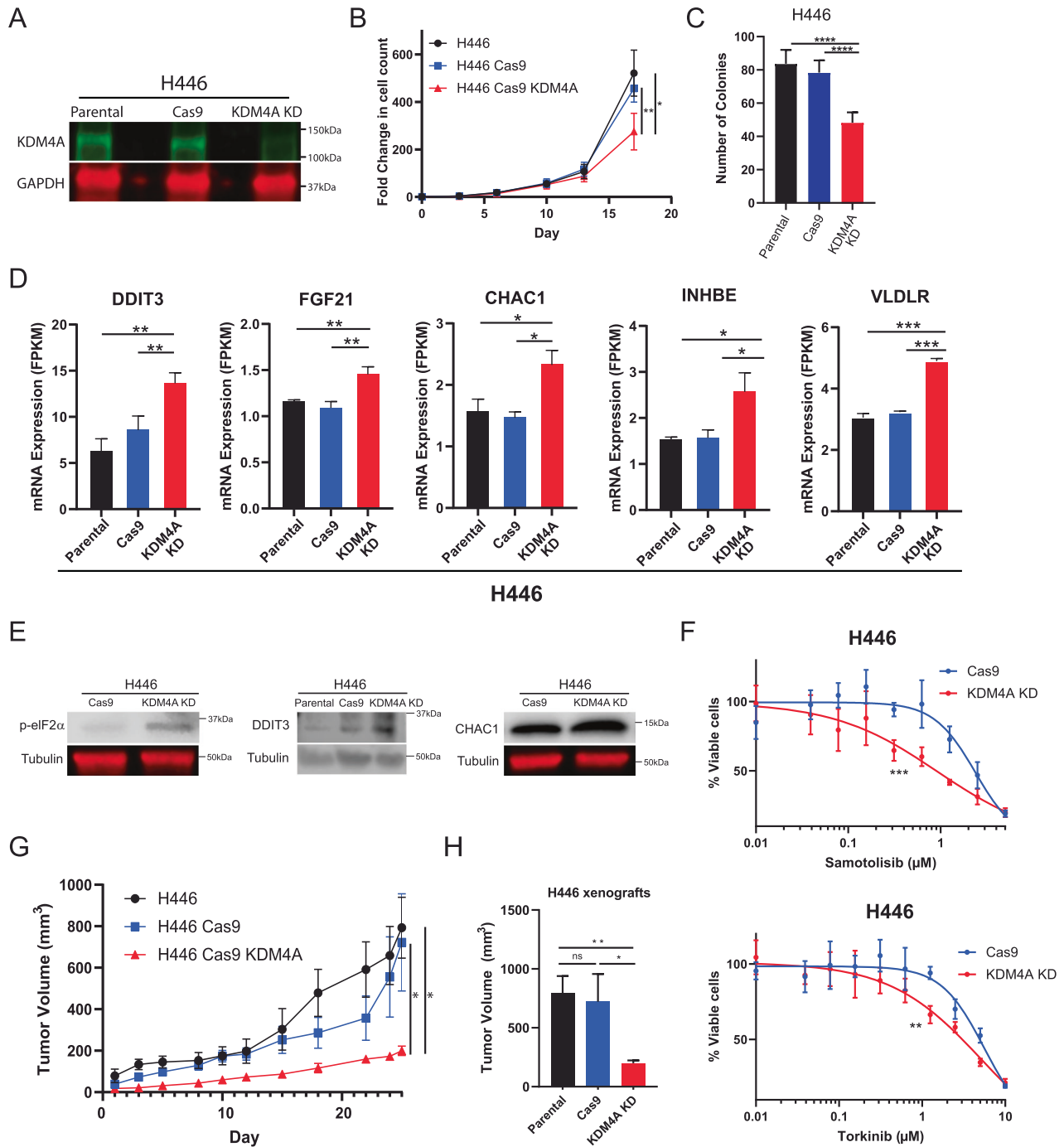
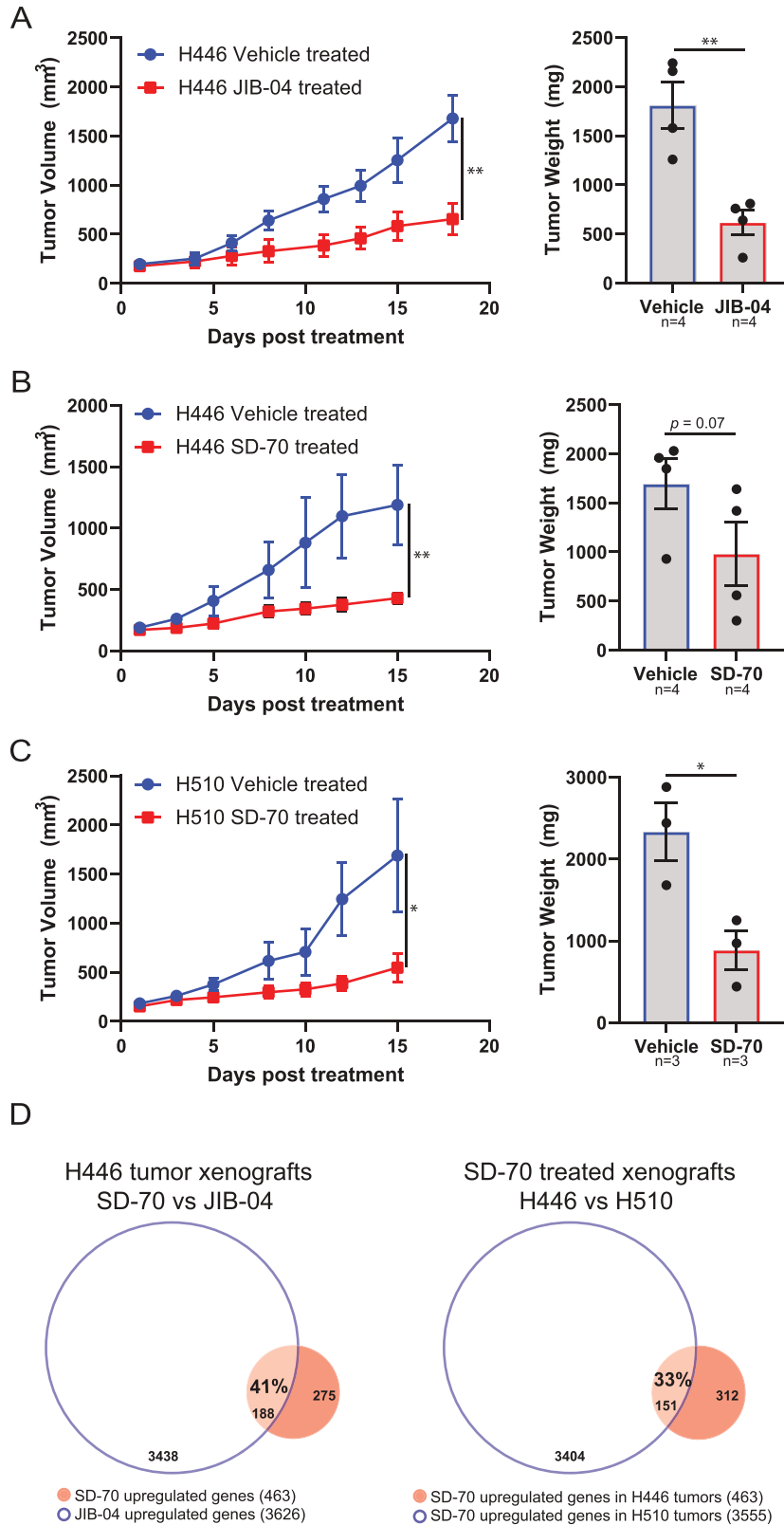


Fig. 5 Depletion of the ER stress transcriptional regulator Jumonji KDM4A upregulates ER stress and mTOR signaling, decreases cell proliferation in vitro, and blunts tumor growth in vivo. **A** Immunoblot demonstrating decrease of KDM4A (top) in H446 cells compared to parental and Cas9-only control cells. GAPDH (bottom) was used as the loading control. **B** Loss of KDM4A in H446 decreases proliferation compared to parental and Cas9-only H446 cells. See the methods section for experimental details. Error bars represent SD from the mean across 4–5 biological replicates. $** = p \leq 0.01$, $* = p \leq 0.05$, by two-tailed *t*-test, unequal variance. **C** Depletion of KDM4A in H446 decreases colony formation potential compared to parental and Cas9-only H446 cells. Each colony is defined by a cluster of approximately 100 cells. Error bars are SEM across six replicates. $**** = p \leq 0.0001$ by two-tailed *t*-test, unequal variance. **D** Upregulation of ER stress pathway genes measured by RNA-sequencing in KDM4A knockdown compared to parental and Cas9-only H446 cells. Data are shown as mean \pm SD, $n = 3$. $*** = p \leq 0.001$, $** = p \leq 0.01$, $* = p \leq 0.05$, by two-tailed *t*-test, unpaired with Welch's correction. **E** ER stress proteins p-eIF2 α , DDIT3, and CHAC1 are upregulated in H446 KDM4A knockdown cells vs controls, as shown by Western blot. Tubulin is a loading control. **F** MTS viability curves of H446 Cas9 vs KDM4A knockdown cells in response to mTOR inhibitors. Data are average \pm SD for each dose, $n = 4$. *P*-values for curve comparisons calculated by GraphPad Prism (top, bottom, IC₅₀, Hill coefficient). **G** Growth of cell line-derived xenografts in nude mice demonstrates suppressed tumor progression in H446 tumors with KDM4A knockdown compared to controls. Data are shown as mean \pm SEM. H446 parental ($n = 5$), H446 Cas9 ($n = 6$), H446 Cas9 KDM4A ($n = 7$) and $* = p \leq 0.05$, by one-tailed *t*-test, unequal variance. **H** Bar graph representing final tumor volumes in H446 xenografts. H446 KDM4A knockdown xenograft volumes were significantly lower compared to parental and Cas9-only controls. Data are shown as means \pm SEM. $** = p \leq 0.01$, $* = p < 0.05$, by one-tailed *t*-test, unpaired with Welch's correction.



inhibitor TACH101 [36] currently open for the first time (NCT05076552), the translation of our findings to the clinical setting may be within the foreseeable future not only for SCLC but also for other tumor types, particularly those that lack functional RB1. Major translational and mechanistic questions emerge from

this work, including whether Jumonji inhibitors would be most effective when paired with chemotherapy in the first-line setting, as consolidation therapy after response to chemotherapy, or as a treatment for relapsed resistant SCLC as well as their mode of action in potentially targeted oncogenic protein downregulation.

Fig. 6 KDM4 inhibitors decrease the growth rate of H446 and H510 cell line-derived xenograft tumors in vivo and regulate common genes. A Growth of H446 xenograft tumors grown in nude mice is significantly suppressed after treatment with JIB-04. Tumor weight was likewise significantly decreased in JIB-04-treated mice. JIB-04 was given via oral gavage three times a week (Mon, Wed, Fri) at 75 mg/kg. Data are shown as mean \pm SEM ($n = 4$ per treatment group). **B** Growth of H446 xenograft tumors grown in nude mice was suppressed after treatment with SD70. Tumor weight decreased in SD70-treated animals, showing a nearly significant trend. SD70 was given by IP injection Mon-Fri at 10 mg/kg. Data are shown as mean \pm SEM ($n = 4$ per treatment group). **C** Growth of H510 xenograft tumors grown in nude mice is significantly suppressed after treatment with SD70. Tumor weight was significantly decreased in SD70-treated animals. Data are shown as mean \pm SEM ($n = 3$ per treatment group). ** = $p \leq 0.01$, * = $p \leq 0.05$, by two-tailed *t*-test, unequal variance. **D** Venn diagrams depicting the overlap in upregulated genes (≥ 1.5 over vehicle) between JIB-04 and SD70 in H446 xenografts (left panel, $n = 3$ per treatment group) and between SD70-treated H446 vs H510 xenografts ($n = 3$ per xenograft).

MATERIALS AND METHODS

Cell lines

SCLC cell lines from the Hamon Center Collection (University of Texas Southwestern Medical Center) were DNA fingerprinted using PowerPlex 1.2 kit (Promega) and tested for mycoplasma using e-Myco kit (Boca Scientific). Cell lines used in this study (Table 1) were maintained in RPMI-1640 (Life Technologies Inc.) with 5% FBS at 37 °C in a humidified atmosphere containing 5% CO₂.

In vitro viability assays

The number of cells plated per well were optimized (Supplementary Information, Supplementary Table 1) for readout in 96-well plates. Drugs were tested in serial dilutions, totaling 9 different drug concentrations, with 4–8 replicates per concentration. Response was validated in independent plates ($n \geq 2$). Cell viability after 4-day treatments was assessed using standard MTS assays (Promega, G1111) according to the manufacturer's instructions. The soluble formazan product was measured by relative absorbance. JIB-04 E isomer was synthesized in-house as originally described [32]. SD70 was from Xcess Biosciences (M6194), GSK-J4 from Tocris (4594), etoposide was from APP (100425), Torkinib from MCE (HY-10474), Samotolisib was from MCE (HY-12513) and TACH101 from ProbeChem (PC-72259).

RNA-sequencing

For RNA-seq, cell lines were plated at a density of 4×10^6 cells per 10 cm² plate and allowed to rest overnight. Cells were then treated with the indicated inhibitor dose for 24 h and harvested. For the experiment with the H446, H446 Cas9, and H446 Cas9 KDM4A series, 4×10^6 cells were plated into 10 cm² plates and allowed to rest for ~12 h overnight and collected. RNA extraction from cells was carried out using the RNeasy Plus Mini Kit (Qiagen, 74134). RNA from tumors was extracted using Trizol (ThermoFisher Scientific, 15596018). Quality scores (QC) were checked before RNA-sequencing (Novogene, 30 M raw paired reads, NovaSeq 6000 or HiSeq X Ten). Fastq files were aligned to the GRCh38 human reference genome using STAR v2.7.1a. The bam files were processed to remove read duplicates using Picard MarkDuplicates from GATK v4.1.2. FPKM values were obtained using Cufflinks v2.2.1. FPKM values were upper-quartile normalized, then log-transformed. The tab-limited text files included log₂FPKM values for each sample. Pathway enrichment was analyzed using Gene Set Enrichment Analysis or TOPPGene online tools [57]. Differential analysis was a comparison between DMSO-treated cells to drug-treated cells or H446 Cas9 versus H446 KDM4A knockdown cells. NE scores were determined as previously described [27]. Briefly, an RNA expression signature was generated from normal adrenal medulla (NE) compared to normal adrenal cortex (non-NE) and then applied to lung cancer cell lines to generate a new lung cancer-specific 50-gene NE expression signature. An NE score formula (using a nearest-neighbor approach) was then derived from this lung NE signature so that any lung sample can be graded on a -1 (non-NE) to +1 (NE) scale.

Gene ontology analysis and KDM4A target genes

GSEA analysis for Fig. 3A was done using mTORC1 signaling genes from Hallmark M5924 using HUGO symbols. ER stress genes were compiled from [37–42] and the following GSEA processes using HUGO symbols: M23457, M42756, M22993, M10426, M14363, M34313, M25210, M13959, M25208, M45871, M11965, M42776, M15498, M39878, M1477, M5922, M10294 and duplicates removed. KDM4A target genes used to generate the Venn Diagram in Fig. 5C were obtained from ChIP Atlas (H sapiens (hg38), ± 5 Kb from TSS of hESC: SRX116463|hESC_H1 and SRX186675|hESC_H1, with the cut off at 300 or greater) [58, 59] and from KDM4A transgenic and

knockout models based on genes with HUGO symbols [31]. For KDM4A target genes used to generate the Venn Diagram in Fig. 5B, H446 KDM4A KD-regulated genes were included along with the ChIP Atlas data based on genes with HUGO symbols. For Fig. 6D, gene symbols were used in all the analyses. NOTCH pathway genes shown in the RNA-seq dataset tab for Fig. 7 are from GSEA M39540 (HUGO symbols).

Western blots

Cells were plated at a density of 4×10^6 cells per 10 cm² culture dish. Cells were rinsed with 1 \times PBS, trypsinized, then washed with cold 1 \times PBS before lysing with RIPA buffer (50 mM Tris, 150 mM NaCl, 0.1% SDS, 1% IGEPAL CA-630, 1% sodium deoxycholate, 2 mM MgCl₂, pH 8) with 1 unit/ μ L benzonase (Millipore–Sigma, E1014), protease inhibitors (Millipore–Sigma, P8340) and phosphatase inhibitors (Millipore–Sigma, 4906845001). Supernatants were collected after spinning at max speed for 10 min. Protein quantification was done using BCA kit (ThermoFisher Scientific, 23225) or using the Lowry Protein Assay kit (BioRad, 5000112). Samples were mixed with 4X Laemmli buffer (BioRad, 161-0747) and 2-Mercaptoethanol (ThermoFisher Scientific, 2198023) then boiled before loading 20–100 μ g of protein on a 4–20% Mini-PROTEAN TGX gel (BioRad, 4561096) for ~2 h at 75 V or 1 h at 130 V. Protein was transferred using the Trans-Blot Turbo RTA Mini Nitrocellulose transfer kit (Biorad, 1704270) on the Trans-Blot Turbo Transfer System (Biorad, 1704150) using manufacturers suggested protocol. For blocking and diluting antibodies, 5% milk or BSA was used. Secondary antibodies were used based on the primary antibody. Revert 700 Total Protein Stain (LICOR, 926-11021) was used to normalize protein band signals that lacked a true loading control (Fig. 7E and Fig. 7A). Images were acquired using LICOR Odyssey Fc Imager. Some proteins were detected with fluorescence and may be shown pseudo-colored in a gray scale.

Tumors were weighed then lysed with RIPA buffer supplemented with protease and phosphatase inhibitors: 10 μ l of lysis buffer per mg of tumor. Tumors were homogenized using tissue lyzer (Qiagen Tissuelyzer II) applying two rounds (60 s/round) for each sample. Samples were then sonicated, performing three rounds (5 s/round). Then samples were centrifuged at 15,000 rpm for 10 min at 4 °C. Protein concentrations were determined and prepared for western blotting as described above. Nuclear extracts of tumors were prepared as described under the “Histone demethylase activity assays” section below. For primary and secondary antibodies used for Western blots see Supplementary Table 2.

Annexin V assays

Cells were plated at a density of 3.4×10^5 cells per well in a 6-well plate. The next day, cells were treated with JIB-04 or SD70 at their respective IC₅₀ doses for 48 h or 72 h then harvested and stained for Annexin V using the FITC Annexin V Apoptosis Detection Kit I (BD Biosciences, 556547) according to the manufacturer's instruction. The IC₅₀ doses of JIB-04 for H446, H2171, H524, and H510 were 0.04 μ M, 0.45 μ M, 0.49 μ M, and 0.02 μ M, respectively. The IC₅₀ doses of SD70 for H446, H2171, H524, and H510 were 1.2 μ M, 2.1 μ M, 2.25 μ M, and 2.2 μ M, respectively. Experiments were done in triplicate. Samples were co-stained with propidium iodide and analyzed by the UT Southwestern Flow and Mass Cytometry Facility. Data was acquired on a Becton Dickinson FACSAria II, using DIVA software. It was then analyzed using Flowjo software version 10.10.0. Cells were gated on FSC vs SSC to exclude debris and then fluorescence gates were based on single color controls.

Mass spectrometry sample preparation and data analysis

H446 cells were plated at a density of 4×10^6 cells per 10 cm² culture dish. H446 cells were treated with IC₅₀ doses of JIB-04 (0.04 μ M) and SD70

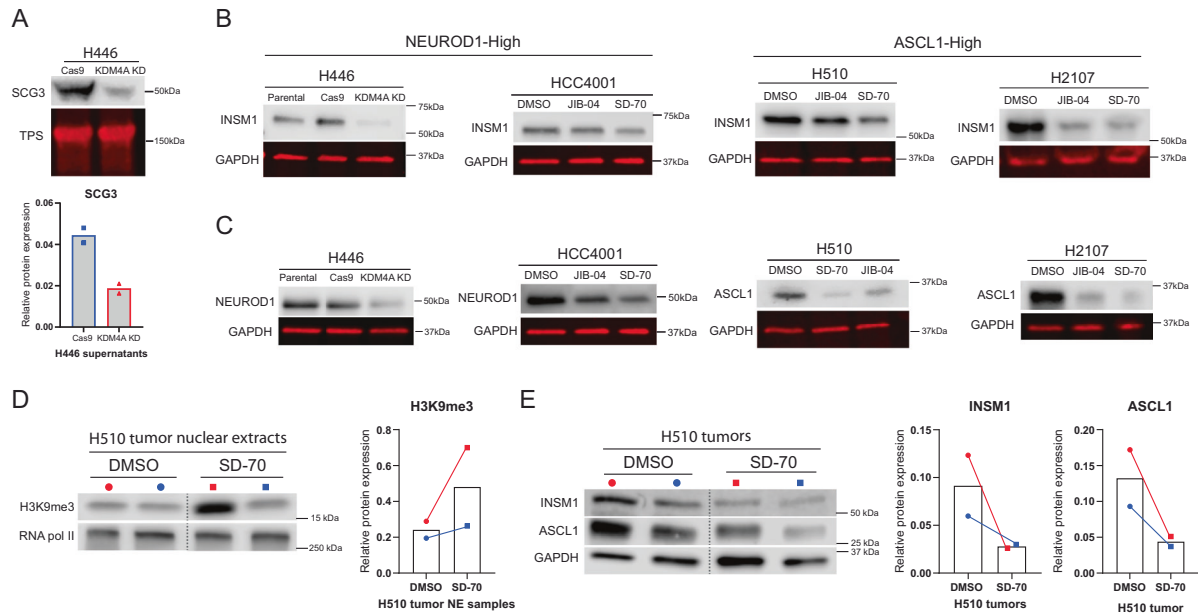


Fig. 7 Jumonji inhibition or KDM4A genetic knockdown alter the protein levels of key modulators of small cell lung cancer phenotypes in cells and in vivo. **A** The SCLC marker Secretogranin-3 is decreased in KDM4A knockdown cell secreted media compared to Cas9 control H446 cells. A representative immunoblot is shown along with a section of total protein stain for the same gel. Quantification across two independent experiments normalized to total protein lysate is shown in the bar graph. **B** Western analysis validates the downregulation of INSM1 protein expression in H446 KDM4A KD cells, as well as in HCC4001, H510, and H2107 cells treated with Jumonji inhibitors, as indicated. GAPDH was used as a loading control. **C** NEUROD1 or ASCL1 Western blots show decreased protein in KDM4A KD or SD70 and JIB-04 treated cells. NEUROD1-high (H446, HCC4001) and ASCL1-high cells (H510, H2107) cells are shown. GAPDH as loading control. Note that in some cases the same gels were used to probe for INSM1 and NEUROD1 or ASCL1 thus sharing the same loading control. Quantifications are given in Fig. S7. **D** Western blots showing upregulation of H3K9me3 levels in H510 tumor nuclear extracts ($n = 2$ per treatment group) with RNA polymerase II used as a loading control. Quantification is shown on the right with lines connecting the DMSO control and SD70-treated mouse pairs. **E** Western blots showing decreased INSM1 and ASCL1 protein levels in H510 tumor lysates ($n = 2$ per treatment group) with GAPDH as a loading control. Quantifications are shown on the right with lines connecting DMSO control and SD70-treated mouse pairs. **D, E** dotted lines represent the place in the membrane where an extra control lane between DMSO and drug-treated samples was removed for simplicity of presentation.

(1.2 μM) for 24 h. H446 parental, Cas9, and KDM4A knockdown (KD) cells were plated, grown, and collected in tandem with H446 treated cells. Samples were prepared in duplicate. Cells were lysed according to the steps used for western blotting. Samples were then sent to UT Southwestern Proteomics Core for LC-MS/MS protein identification. Trypsin digests of lysate samples were run on an Orbitrap Fusion Lumos nanoLC-MS/MS system (Thermo) and were analyzed using Proteome Discoverer v.2.4 (Thermo) searching against the human-reviewed protein database from UniProt.

Raw data represented the abundance of each detectable protein in the whole cell lysates. Only values labeled with high confidence were used for analysis. Abundance of each protein was normalized to the total abundance for all samples. Fold-change ratios (JIB-04/DMSO, SD70/DMSO, KDM4A KD/Cas9) were used to analyze changes in protein expression. Downregulated proteins were defined as those whose fold change for treatment was ≤ 0.5 and ≤ 0.7 for the other two treatments.

Histone demethylase activity assays

H446 and H2171 cell lines were plated at a density of 12×10^6 cells per 150 mm^2 plate (Corning, 430599). The cells were then treated with JIB-04 and SD70 IC_{50} . Cells were collected 24 h after treatment, washed with $1 \times$ PBS, and flash frozen. Nuclear extracts were prepared using Epigentek kit (OP-0002-1). For H2171 cells, PBS lysates were prepared in addition to the nuclear extracts by resuspending the cell pellets in $400 \mu\text{l}$ of $1 \times$ PBS supplemented with phosphatase inhibitors (Roche, 04-906-837-001) and EDTA-free protease inhibitors (Roche, 05-892-791-001) and sonicated at 5% power 3 times 10 s each round with 30 s rest between rounds. Demethylase activity was determined using Epigenase JMJD2 Demethylase Activity/Inhibition Assay Kit (P-3081). For H446 cells, nuclear extracts were used as the enzyme source for the demethylase reaction with $100 \mu\text{M}$

Fe(II), 1 mM α -ketoglutarate, and 2 mM ascorbate. For H2171 cells, both nuclear extracts and PBS lysates were used as the enzyme source for the demethylase reaction with similar conditions as H446 except that $10 \mu\text{M}$ Fe(II) was used.

Generation of knockdown cell lines

For cell lines with stable knockout of KDM4A or KDM5B, HEK293T cells (Clontech) were transfected with FuGENE6 (Promega), pMD2-VSV-G packaging plasmid (Addgene), pCMV-dR8.2 envelope plasmid (Addgene) and Edit-R Cas9 plasmid (Dharmacon). Viruses were harvested and filtered 1- and 2 days post-transfection. SCLC lines were plated into 6-well plate (Corning, 3516) and infected with the virus. Cells were then selected with Blasticidin (Gibco) at a predetermined concentration for 7 days. This yielded stable Cas9-expressing cell lines. gRNA targeting KDM4A or KDM5B (Millipore-Sigma) virus were generated using the same protocol. Cas9 cell lines were plated into 6-well plate and infected with virus. Cells were then selected with puromycin (Invitrogen) at a predetermined concentration for 7 days. For cell lines with an inducible knockout of KDM4A or KDM5B Clontech Lenti-HEK293FT cells were transfected with FUGENE6, pCMV-dR8.91 (packaging), pMD2-VSV-G (envelope) and Inducible Edit-R Cas9 plasmid (Dharmacon). Virus was harvested and filtered 1- and 2 days post-transfection. H1522 cells were plated at a density of 1.0×10^6 cells in a well of a 6-well plate and left to rest for 24 h. H1522 cells were then infected with the Cas9 virus by centrifuging the cells at a low speed with the lentivirus overnight. Cells were then selected with blasticidin (Gibco) at a predetermined concentration to yield cells expressing inducible Cas9. H1522 Inducible Cas9 cells were plated at a density of 1.5×10^6 cells per 10 cm^2 plate and infected with the gKDM4A lentivirus. Cells were then selected with puromycin (Invitrogen). For cell maintenance during culturing, in all cases, $0.25 \mu\text{g/mL}$ puromycin and $4 \mu\text{g/mL}$ blasticidin were

used. Cas9 expression was induced with 1 µg/mL doxycycline for 48–72 h before the start of experiments, as indicated in legends.

Proliferation assays

For long-term proliferation assays, H446, H446 Cas9, and H446 Cas9 KDM4A or Cas9 KDM5B cell lines were plated at a density of 260,000 cells per 10 cm² plate. Cells were then counted (Beckman Coulter Z2) every 3–4 days and re-plated at lower density onto new plates until day 17 is reached. To calculate fold change, cell counts were divided by the cell count of day 0. For short-term (<7 days) proliferation assays, H524 Cas9, and KDM4A KD cells were plated on multiple plates at a density of 25,000 cells per well in a 96-well plate with 4 replicates per cell line. H1522 Cas9 and KDM4A KD cells were treated with 1 µg/ml doxycycline for 48 h before plating for the proliferation assay. Cells were kept on doxycycline treatment throughout duration of the assay and were plated at a density of 5000 cells per well in multiple 96-well plates with 4 replicates per cell line. Cell viability was measured over a time course of multiple days using manufacturer's instructions for MTS assay. The soluble formazan product was measured by relative absorbance and optical densities were blank-corrected. Days 2–4 and 4–6 are displayed in Fig S5J for H524 and H1522 cell lines, respectively.

Colony formation assay

H446, H446 Cas9, and H446 Cas9 KDM4A cell lines were plated into 6-wells plates (250 cells/well, Corning, 3516). The cells were then allowed to grow for 14 days with media being changed every 3–4 days. On day 14, wells were stained with 0.5% crystal violet (Sigma, C-3886-25G) in 3% formaldehyde (Sigma, F-1268). Wells were then allowed to dry overnight. Colonies were then counted blindly. ~100-cells cluster were considered one colony.

Development of murine xenografts and investigation of Jumonji inhibitors in vivo

H446, H446 Cas9, and H446 Cas9 KDM4A cell lines were plated into six 175 cm² flasks and grown to 75% confluence (Corning, 07-202-000). Five million cells in 100 µl PBS were injected subcutaneously into the right flank of each mouse. Tumor length and width were measured thrice weekly and volumes were calculated using (L²*W)/2.

H446 and H510 cell lines were plated into eight 175 cm² flasks and grown to 75% confluence. Five million H446 cells in 100 µl 1× PBS were injected subcutaneously into the right flank of each mouse. These tumors were allowed to grow to 150–200 mm³ then JIB-04 or control treatment were given three times a week via oral gavage at 75 mg/kg as before [29, 30]. Tumor length and width were measured thrice weekly, and volumes were calculated using (L²*W)/2. Another set of mice were injected with H446 on the right flanks in a similar manner; in these mice, 3 × 10⁶ H510 cells were also injected into the left flanks. These tumors were allowed to grow to 150–200 mm³ then mice were paired by tumor volume and treated M-F with SD70 (from a DMSO dissolved stock diluted into 75% of PEG300, 25% of 5% dextrose water) via IP injection at 10 mg/kg or vehicle [60]. Tumors length and width were measured three times a week and volumes were calculated using (L²*W)/2. All mouse studies were conducted under UTSW IACUC approval.

DATA AVAILABILITY

All data will be deposited publicly and made available and all reagents will be shared with the scientific community. RNA-seq data of untreated SCLC cells has been deposited at dbGaP under accession #phs001823.v1.p1. RNA-seq data of the H446 genetic series and of treated cells has been deposited at GEO (GSE208446).

REFERENCES

- Gazdar AF, Bunn PA, Minna JD. Small-cell lung cancer: what we know, what we need to know and the path forward. *Nat Rev Cancer*. 2017;17:765.
- Wang S, Tang J, Sun T, Zheng X, Li J, Sun H, et al. Survival changes in patients with small cell lung cancer and disparities between different sexes, socioeconomic statuses and ages. *Sci Rep*. 2017;7:1339.
- Cai L, Liu H, Huang F, Fujimoto J, Girard L, Chen J, et al. Cell-autonomous immune gene expression is repressed in pulmonary neuroendocrine cells and small cell lung cancer. *Commun Biol*. 2021;4:314.
- Petty WJ, Paz-Ares L. Emerging strategies for the treatment of small cell lung cancer: a review. *JAMA Oncol*. 2023;9:419–29.

- Brahmer JR, Lee JS, Ciuleanu TE, Bernabe Caro R, Nishio M, Urban L, et al. Five-year survival outcomes with nivolumab plus ipilimumab versus chemotherapy as first-line treatment for metastatic non-small-cell lung cancer in CheckMate 227. *J Clin Oncol*. 2023;41:1200–12.
- Paz-Ares L, Chen Y, Reinmuth N, Hotta K, Trukhin D, Stastenko G, et al. Durvalumab, with or without tremelimumab, plus platinum-etoposide in first-line treatment of extensive-stage small-cell lung cancer: 3-year overall survival update from CASPIAN. *ESMO Open*. 2022;7:100408.
- Borromeo MD, Savage TK, Kollipara RK, He M, Augustyn A, Osborne JK, et al. ASCL1 and NEUROD1 reveal heterogeneity in pulmonary neuroendocrine tumors and regulate distinct genetic programs. *Cell Rep*. 2016;16:1259–72.
- Borges M, Linnoila RI, van de Velde HJ, Chen H, Nelkin BD, Mabry M, et al. An achaete-scute homologue essential for neuroendocrine differentiation in the lung. *Nature*. 1997;386:852–5.
- Huang YH, Klingbeil O, He XY, Wu XS, Arun G, Lu B, et al. POU2F3 is a master regulator of a tuft cell-like variant of small cell lung cancer. *Genes Dev*. 2018;32:915–28.
- McCull K, Wildey G, Sakre N, Lipka MB, Behtaj M, Kresak A, et al. Reciprocal expression of INSM1 and YAP1 defines subgroups in small cell lung cancer. *Oncotarget*. 2017;8:73745–56.
- Westerman BA, Breuer RH, Poutsma A, Chhatta A, Noorduy LA, Koolen MG, et al. Basic helix-loop-helix transcription factor profiling of lung tumors shows aberrant expression of the proneural gene atonal homolog 1 (ATOH1, HATH1, MATH1) in neuroendocrine tumors. *Int J Biol Markers*. 2007;22:114–23.
- Rudin CM, Poirier JT, Byers LA, Dive C, Dowlati A, George J, et al. Molecular subtypes of small cell lung cancer: a synthesis of human and mouse model data. *Nat Rev Cancer*. 2019;19:289–97.
- Meijer JJ, Leonetti A, Airo G, Tiseo M, Rolfo C, Giovannetti E, et al. Small cell lung cancer: novel treatments beyond immunotherapy. *Semin Cancer Biol*. 2022;86:376–85.
- Polley E, Kunkel M, Evans D, Silvers T, Delosh R, Laudeman J, et al. Small cell lung cancer screen of oncology drugs, investigational agents, and gene and microRNA expression. *J Natl Cancer Inst*. 2016;108:1–11.
- Morabito A, Carillio G, Daniele G, Piccirillo MC, Montanino A, Costanzo R, et al. Treatment of small cell lung cancer. *Crit Rev Oncol Hematol*. 2014;91:257–70.
- Hartwell D, Jones J, Loveman E, Harris P, Clegg A, Bird A. Topotecan for relapsed small cell lung cancer: a systematic review and economic evaluation. *Cancer Treat Rev*. 2011;37:242–9.
- Huffman K, Martinez ED. Pre-clinical studies of epigenetic therapies targeting histone modifiers in lung cancer. *Front Oncol*. 2013;3:235.
- Bayo J, Dalvi MP, Martinez ED. Successful strategies in the discovery of small-molecule epigenetic modulators with anticancer potential. *Future Med Chem*. 2015;7:2243–61.
- Thinness CC, England KS, Kawamura A, Chowdhury R, Schofield CJ, Hopkinson RJ. Targeting histone lysine demethylases — progress, challenges, and the future*. *Biochim Biophys Acta*. 2014;1839:1416–32.
- Zhang L, Chen Y, Li Z, Lin C, Zhang T, Wang G. Development of JmjC-domain-containing histone demethylase (KDM2-7) inhibitors for cancer therapy. *Drug Discov Today*. 2023;28:103519.
- Das ND, Niwa H, Umehara T. Chemical inhibitors targeting the histone lysine demethylase families with potential for drug discovery. *Epigenomes*. 2023;7:7–14.
- McDonald ER 3rd, de Weck A, Schlabach MR, Billy E, Mavrakis KJ, Hoffman GR, et al. Project DRIVE: a compendium of cancer dependencies and synthetic lethal relationships uncovered by large-scale, deep RNAi screening. *Cell*. 2017;170:e510.
- Tsherniak A, Vazquez F, Montgomery PG, Weir BA, Kryukov G, Cowley GS, et al. Defining a cancer dependency map. *Cell*. 2017;170:564–76.e516.
- Oser MG, Sabet AH, Gao W, Chakraborty AA, Schinzel AC, Jennings RB, et al. The KDM5A/RBP2 histone demethylase represses NOTCH signaling to sustain neuroendocrine differentiation and promote small cell lung cancer tumorigenesis. *Genes Dev*. 2019;33:1718–38.
- George J, Lim JS, Jang SJ, Cun Y, Ozretic L, Kong G, et al. Comprehensive genomic profiles of small cell lung cancer. *Nature*. 2015;524:47–53.
- Tlemsani C, Pongor L, Elloumi F, Girard L, Huffman KE, Roper N, et al. SCLC-CellMiner: a resource for small cell lung cancer cell line genomics and pharmacology based on genomic signatures. *Cell Rep*. 2020;33:108296.
- Zhang W, Girard L, Zhang YA, Haruki T, Papari-Zareei M, Stastny V, et al. Small cell lung cancer tumors and preclinical models display heterogeneity of neuroendocrine phenotypes. *Transl Lung Cancer Res*. 2018;7:32–49.
- Bayo J, Fiore EJ, Dominguez LM, Real A, Malvicini M, Rizzo M, et al. A comprehensive study of epigenetic alterations in hepatocellular carcinoma identifies potential therapeutic targets. *J Hepatol*. 2019;71:78–90.
- Bayo J, Tran TA, Wang L, Pena-Llopis S, Das AK, Martinez ED. Jumonji inhibitors overcome radioresistance in cancer through changes in H3K4 methylation at double-strand breaks. *Cell Rep*. 2018;25:1040–50.e1045.

30. Dalvi MP, Wang L, Zhong R, Kollipara RK, Park H, Bayo J, et al. Taxane-platin-resistant lung cancers co-develop hypersensitivity to JumoniC demethylase inhibitors. *Cell Rep.* 2017;19:1669–84.
31. Tran TA, Zhang QJ, Wang L, Gonzales C, Girard L, May H, et al. Inhibition of Jumoni demethylases reprograms severe dilated cardiomyopathy and prolongs survival. *J Biol Chem.* 2022;298:101515.
32. Wang L, Chang J, Varghese D, Dellinger M, Kumar S, Best AM, et al. A small molecule modulates Jumoni histone demethylase activity and selectively inhibits cancer growth. *Nat Commun.* 2013;4:2035.
33. Kitajima S, Sun W, Lee KL, Ho JC, Oyadomari S, Okamoto T, et al. A KDM6 inhibitor potently induces ATF4 and its target gene expression through HRI activation and by UTX inhibition. *Sci Rep.* 2021;11:4538.
34. Ku HC, Cheng CF. Master regulator activating transcription factor 3 (ATF3) in metabolic homeostasis and cancer. *Front Endocrinol.* 2020;11:556.
35. Kennedy D, Samali A, Jager R. Methods for studying ER stress and UPR markers in human cells. *Methods Mol Biol.* 2015;1292:3–18.
36. Chandhasin C, Dang V, Perabo F, Del Rosario J, Chen YK, Filvaroff E, et al. TACH101, a first-in-class pan-inhibitor of KDM4 histone demethylase. *Anticancer Drugs.* 2023;34:1122–31.
37. Lee HA, Chu KB, Moon EK, Quan FS. Glutathione peroxidase 8 suppression by histone deacetylase inhibitors enhances endoplasmic reticulum stress and cell death by oxidative stress in hepatocellular carcinoma cells. *Antioxidants.* 2021;10:1503–21.
38. Crawford RR, Prescott ET, Sylvester CF, Higdon AN, Shan J, Kilberg MS, et al. Human CHAC1 protein degrades glutathione, and mRNA induction is regulated by the transcription factors ATF4 and ATF3 and a bipartite ATF/CRE regulatory element. *J Biol Chem.* 2015;290:15878–91.
39. Mungrue IN, Pagnon J, Kohannim O, Gargalovic PS, Lusis AJ. CHAC1/MGC4504 is a novel proapoptotic component of the unfolded protein response, downstream of the ATF4-ATF3-CHOP cascade. *J Immunol.* 2009;182:466–76.
40. Maruyama R, Shimizu M, Hashidume T, Inoue J, Itoh N, Sato R. FGF21 alleviates hepatic endoplasmic reticulum stress under physiological conditions. *J Nutr Sci Vitaminol.* 2018;64:200–8.
41. Dombroski BA, Nayak RR, Ewens KG, Ankeney W, Cheung VG, Spielman RS. Gene expression and genetic variation in response to endoplasmic reticulum stress in human cells. *Am J Hum Genet.* 2010;86:719–29.
42. Martin L, Gardner LB. Stress-induced inhibition of nonsense-mediated RNA decay regulates intracellular cystine transport and intracellular glutathione through regulation of the cystine/glutamate exchanger SLC7A11. *Oncogene.* 2015;34:4211–8.
43. Szeitz B, Megyesfalvi Z, Woldmar N, Valko Z, Schwendenwein A, Barany N, et al. In-depth proteomic analysis reveals unique subtype-specific signatures in human small-cell lung cancer. *Clin Transl Med.* 2022;12:e1060.
44. Wang XD, Hu R, Ding Q, Savage TK, Huffman KE, Williams N, et al. Subtype-specific secretomic characterization of pulmonary neuroendocrine tumor cells. *Nat Commun.* 2019;10:3201.
45. Togayachi A, Iwaki J, Kaji H, Matsuzaki H, Kuno A, Hirao Y, et al. Glycobiomarker, fucosylated short-form secretogranin III levels are increased in serum of patients with small cell lung carcinoma. *J Proteome Res.* 2017;16:4495–505.
46. Fujino K, Motooka Y, Hassan WA, Ali Abdalla MO, Sato Y, Kudoh S, et al. Insulinoma-associated protein 1 is a crucial regulator of neuroendocrine differentiation in lung cancer. *Am J Pathol.* 2015;185:3164–77.
47. Maleki Z, Nadella A, Nadella M, Patel G, Patel S, Kholova I. INSM1, a novel biomarker for detection of neuroendocrine neoplasms: cytopathologists' view. *Diagnostics.* 2021;11:2172–90.
48. Rudin CM, Brambilla E, Faivre-Finn C, Sage J. Small-cell lung cancer. *Nat Rev Dis Prim.* 2021;7:3.
49. Kawabata S, Connis N, Gills JJ, Hann CL, Dennis PA. Nelfinavir inhibits the growth of small-cell lung cancer cells and patient-derived xenograft tumors. *Anticancer Res.* 2021;41:91–99.
50. McBrayer SK, Olenchok BA, DiNatale GJ, Shi DD, Khanal J, Jennings RB, et al. Autochthonous tumors driven by Rb1 loss have an ongoing requirement for the RBP2 histone demethylase. *Proc Natl Acad Sci USA.* 2018;115:E3741–E3748.
51. Varaljai R, Islam AB, Beshiri ML, Rehman J, Lopez-Bigas N, Benevolenskaya EV. Increased mitochondrial function downstream from KDM5A histone demethylase rescues differentiation in pRB-deficient cells. *Genes Dev.* 2015;29:1817–34.
52. Crabtree JS, Singleton CS, Miele L. Notch signaling in neuroendocrine tumors. *Front Oncol.* 2016;6:94.
53. Gazdar AF, Bunn PA, Minna JD. Small-cell lung cancer: what we know, what we need to know and the path forward. *Nat Rev Cancer.* 2017;17:725–37.
54. Tang N, Xu S, Song T, Qiu Y, He J, Fu X. Zinc finger protein 91 accelerates tumour progression by activating beta-catenin signalling in pancreatic cancer. *Cell Prolif.* 2021;54:e13031.
55. Unoki M, Okutsu J, Nakamura Y. Identification of a novel human gene, ZFP91, involved in acute myelogenous leukemia. *Int J Oncol.* 2003;22:1217–23.
56. Wu W, Nelson GM, Koch R, Donovan KA, Nowak RP, Heavican-Foral TB, et al. Overcoming IMiD resistance in T-cell lymphomas through potent degradation of ZFP91 and IKZF1. *Blood.* 2022;139:2024–37.
57. Chen J, Xu H, Aronow BJ, Jegga AG. Improved human disease candidate gene prioritization using mouse phenotype. *BMC Bioinform.* 2007;8:392.
58. Zou Z, Ohta T, Miura F, Oki S. ChIP-Atlas 2021 update: a data-mining suite for exploring epigenomic landscapes by fully integrating ChIP-seq, ATAC-seq and Bisulfite-seq data. *Nucleic Acids Res.* 2022;50:W175–W182.
59. Oki S, Ohta T, Shioi G, Hatanaka H, Ogasawara O, Okuda Y, et al. ChIP-Atlas: a data-mining suite powered by full integration of public ChIP-seq data. *EMBO Rep.* 2018;19:e46255.
60. Shao N, Cheng J, Huang H, Gong X, Lu Y, Idris M, et al. GASC1 promotes hepatocellular carcinoma progression by inhibiting the degradation of ROCK2. *Cell Death Dis.* 2021;12:253.
61. Subramanian A, Tamayo P, Mootha VK, Mukherjee S, Ebert BL, Gillette MA, et al. Gene set enrichment analysis: a knowledge-based approach for interpreting genome-wide expression profiles. *Proc Natl Acad Sci USA.* 2005;102:15545–50.

AUTHOR CONTRIBUTIONS

AN performed many of the experiments analyzed data, and wrote parts of the manuscript. CN performed cell culture, Western blot, and drug response experiments, analyzed data, and wrote parts of the manuscript. TAT performed enzyme experiments, analyzed multiple datasets, and helped in figure design. LG processed genomic data and performed hierarchical clustering and correlation analysis. MP performed some MTS experiments and provided input. KA performed some Western blots. RC performed some Western blots and cell experiments. CG performed Annexin IV assays with CN. RCh performed aspects of the in vivo work and edited parts of the manuscript. BD provided intellectual input and clinical insights. JDM guided aspects of the work and co-lead the project. EDM guided all aspects of the work, designed and analyzed experiments, co-lead the project, and wrote the manuscript.

FUNDING

This work was supported by the Department of Defense (HT94252310012 to EDM), The Welch Foundation (I-1878 to EDM), the NIH (Lung Cancer SPORE P50 CA070907, U24 CA213274, U01 CA213338, CA142543 to JDM, R03CA273480 to EDM with a diversity supplement to CN), the Cancer Prevention and Research Institute of Texas Training grant (RP160157), and the UT Southwestern TARDIS Physician-Scientist Fellowship, which is funded by the Burroughs-Wellcome Fund (RCh). The authors thank the UT Southwestern Proteomics Core facility for help in performing proteomics experiments and acknowledge the helpful comments of current and former members of the Martinez and Minna laboratories including Dr. Juan Bayo-Fina.

COMPETING INTERESTS

JDM receives royalties from the NIH and UTSW for the distribution of human tumor cell lines. None of the other authors have any competing interests to declare.

ETHICS APPROVAL

All methods were performed in accordance with the relevant guidelines and regulations. All mouse studies were conducted under UTSW IACUC approval 2017-102260.

ADDITIONAL INFORMATION

Supplementary information The online version contains supplementary material available at <https://doi.org/10.1038/s41388-024-03125-x>.

Correspondence and requests for materials should be addressed to Elisabeth D. Martinez.

Reprints and permission information is available at <http://www.nature.com/reprints>

Publisher's note Springer Nature remains neutral with regard to jurisdictional claims in published maps and institutional affiliations.



Open Access This article is licensed under a Creative Commons Attribution-NonCommercial-NoDerivatives 4.0 International License, which permits any non-commercial use, sharing, distribution and reproduction in any medium or format, as long as you give appropriate credit to the original author(s) and the source, provide a link to the Creative Commons licence, and indicate if you modified the licensed material. You do not have permission under this licence to share adapted material derived from this article or parts of it. The images or other third party material in this article are included in the article's Creative Commons licence, unless indicated otherwise in a credit line to the material. If material is not included in the article's Creative Commons licence and your intended use is not permitted by statutory regulation or exceeds the permitted use, you will need to obtain permission directly from the copyright holder. To view a copy of this licence, visit <http://creativecommons.org/licenses/by-nc-nd/4.0/>.

© The Author(s) 2024